J Appl Electrochem (2011) 41:173–181
DOI 10.1007/s10800-010-0221-8

ORIGINAL PAPER

Photoelectrocatalytic activity of bi-layer TiO_2/WO_3 coatings for the degradation of 4-chlorophenol: effect of morphology and catalyst loading

J. Georgieva · S. Sotiropoulos · S. Armyanov · N. Philippidis · I. Poulios

Received: 5 February 2010 / Accepted: 21 September 2010 / Published online: 9 October 2010

Abstract WO_3 and bi-layer WO_3/TiO_2 coatings of different catalyst loadings were electrosynthesized on stainless steel 304 (SS) substrates from acidic aqueous solutions by single-step and consecutive steps potentiostatic cathodic deposition. The resulting WO_3/SS and TiO_2/WO_3/SS photoelectrodes were screened for their photoresponse under ultraviolet (UV) and visible light illumination by photovoltammetry and photoamperometry in sulphate solutions, in the absence and presence of 4-chlorophenol (4-CP). They were also evaluated for bulk photo-oxidation of 4-CP under constant potential, in the voltage range determined on the basis of the photovoltammetric tests. The optimal weight ratio between TiO_2 and WO_3 was also established, ensuring the best performance of these photoelectrodes for the photooxidation of 4-CP under UV and visible light irradiation.

Keywords Tungsten trioxide coatings · Titanium dioxide coatings · Stainless steel · 4-Chlorophenol · Photodegradation

1 Introduction

Heterogeneous photocatalysis has been suggested as an alternative method of hazardous waste treatment [1, 2]. One of the most popular photocatalysts is TiO_2, a wide gap *n*-type semiconductor [3], because of its high photocatalytic activity and chemical stability against photocorrosion. The use of TiO_2 slurries necessitates removal of the photocatalyst by filtration. Replacing the slurries by photoelectrodes, wherein the semiconductor is immobilized on a conducting support, can avoid the filtration step of suspended particles but entails mass transfer and active area limitations. If the photoelectrode is subjected to an external positive bias (in an appropriate electrochemical cell), then the photogenerated electrons are drawn away from the catalyst surface through the external cell circuit, and photogenerated holes are transferred to the electrode surface. In this way, the rate of electron–hole recombination is decreased, and the rate of surface reactions increased. This process is known as electrically enhanced photocatalysis [4–9] or photoelectrocatalysis, which can overcome some of the above-mentioned disadvantages of supported photocatalysts. However, the TiO_2 photocatalysts absorb only UV light, and thus it is now more desirable to develop photocatalysts which exhibit visible light response for practical applications [10, 11]. In that direction, minimizing photogenerated electron–hole recombination rates and expanding semiconductor's useful range of operation into visible light wavelengths are the main targets of research aiming at improving the efficiency of TiO_2-based photocatalysts. For example, doping with lanthanide ions [12–14] or coupling with WO_3 [15–25] is known to suppress electron–hole recombination rates. On the other hand, introduction of a visible light active catalyst, such as WO_3 [15–18, 26–30], improves visible light utilization. Hence, coupling TiO_2 with WO_3 is a strategy for achieving both targets. Electrosynthesis of TiO_2 and electrodeposition of WO_3 have been proposed as an alternative route for the production of plain or mixed coatings on Pt, Au or optically transparent electrodes [17–22, 24, 31, 32] and, more

J. Georgieva (✉) · S. Armyanov
Rostislaw Kaischew Institute of Physical Chemistry, Bulgarian Academy of Sciences, 1113 Sofia, Bulgaria
e-mail: jenia@ipc.bas.bg

S. Sotiropoulos · N. Philippidis · I. Poulios
Department of Chemistry, Aristotle University of Thessaloniki, 54124 Thessaloniki, Greece

recently, on economical and practical stainless steel (SS) substrates too [23, 25, 33–35].

The degradation of CPs in aqueous solution has attracted considerable attention because these compounds are important xenobiotic micropollutants in the environment. One of them, 4-CP is used for the production of dyes, drugs and fungicides, and its degradation using semiconductors (mainly TiO_2) under UV light has been the subject of many investigations [36–41]. The photodegradation of 4-CP is initiated by its attack by photogenerated holes or subsequently produced hydroxyl radicals ($OH^{\bullet}$), on the surface of the semiconductor particles [36, 37]. Photocatalytically active TiO_2 films have been produced by spray techniques [38], chemical vapour deposition [39], spin-coating or dip-coating, and by thermal oxidation of titanium metal [40].

In our previous studies, electrosynthesized TiO_2, WO_3 and bi-layer TiO_2/WO_3 coatings were evaluated for the photooxidation of oxalate, malachite green and 4-CP, during bulk photoelectrolysis at constant potential [23, 25, 35]. It was found that application of an external bias and the use of bi-layer TiO_2/WO_3 both improve the photooxidation of all the tested pollutants with respect to those observed at plain TiO_2 under UV and WO_3 coatings under UV and visible light illumination. However, the effect of the loading of these coatings, as well as of the ratio between TiO_2 and WO_3, and their morphology have not been studied yet. (Note that Krýsa et al. [41] have investigated the effect of layer thickness of particulate TiO_2 photocatalysts in the degradation of oxalic acid.)

In that direction, the aim of this article is to electrosynthesize bi-layer TiO_2/WO_3 coatings of different catalyst loadings and compositions and to compare their morphology and photoelectrocatalytic activity towards the photooxidation of 4-CP.

2 Experimental

2.1 WO_3 electrodeposition and bi-layer TiO_2/WO_3 electrosynthesis/electrodeposition on SS substrates

Stainless steel 304 Silko-Inox (SS) substrates were degreased ultrasonically with acetone and etched in a 1:1 HCl/H_2O mixture for 60 s before the electrochemical preparation of the coatings. Small photoelectrode samples for photovoltammetry and photoamperometry experiments were prepared in a 300-mL three-electrode cell using SS rectangular plates (3 cm^2) as the cathode and a Pt foil as the counter electrode. Larger samples (3 × 10 cm^2) for bulk photoelectrolysis were prepared in a 2-L three-electrode cell with platinized titanium plates as counter electrodes. As a reference electrode, in both cases, we employed a mercurous sulphate $Hg/Hg_2SO_4/H_2SO_4$ (0.5 M) electrode (MSE). An Autolab 30 potentiostat (EcoChemie) with a 20 A booster was used for electrodeposition.

WO_3 was obtained from a bath of pH 1.4 containing 0.025 M Na_2WO_4 ($Na_2WO_4{\cdot}2H_2O$; Merck; pro analysis; >99%), 0.03 M H_2O_2 (30% aqueous solution) and 0.05 M HNO_3 (Riedel, 65%) by potentiostatic cathodic deposition for 30 min at –1.00 V vs. MSE. The electrodeposited film was heated at 350 °C for 30 min for crystallization (monoclinic WO_3, as confirmed by XRD (Fig. 1a). TiO_2 layers were electrosynthesized on top of the already formed WO_3 layers by keeping the WO_3/SS electrode at −2.00 V vs. MSE from a solution of pH 1.4 containing 0.02 M $TiOSO_4$ (Fluka; Assay of Ti (as TiO_2) techn., >29%), 0.03 M H_2O_2 (30% aqueous solution), 0.05 M HNO_3 (Riedel, 65%) and 0.1 M KNO_3 (Merck, pro analysi, >99%) [17–25, 31, 32, 34, 35]. For the preparation of TiO_2 layers with different thicknesses, electrosynthesis was repeated two or three times, with drying steps at 150 °C in between, after which the deposited gel films were heated in air at 400 °C

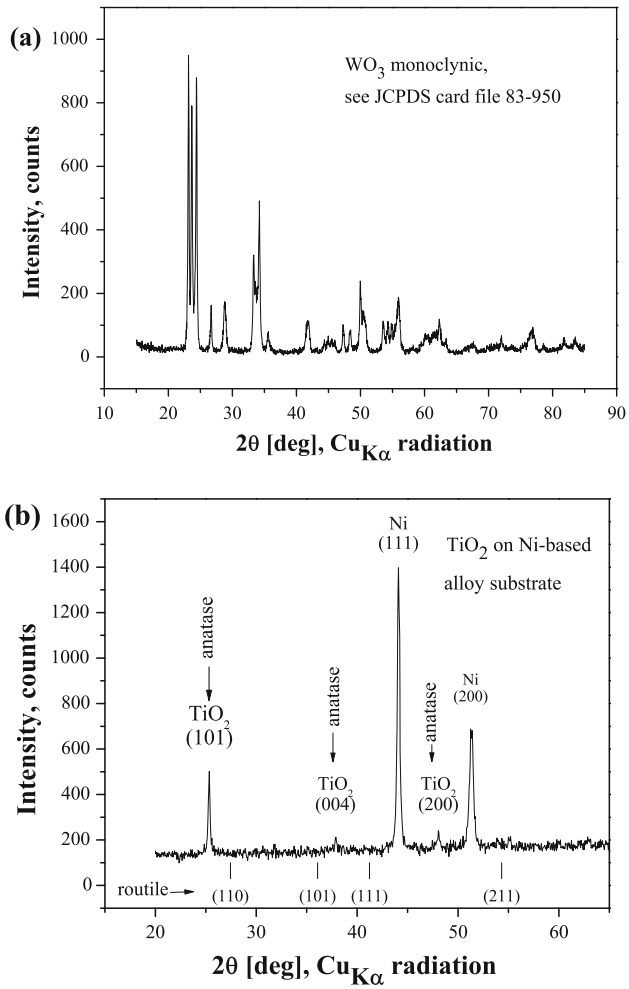

Fig. 1 XRD patterns of WO_3 (**a**) and TiO_2 (**b**) layers after annealing for 1 h at 400 °C

for 1 h to obtain crystalline TiO_2 (anatase, as confirmed by XRD (Fig. 1b) film.

The small photoelectrodes (3 cm^2) tested in this study had loadings 0.30 TiO_2/0.80 WO_3 mg cm^{-2} (Ti:W atomic ratio = 1.1), 0.40 TiO_2/0.70 WO_3 mg cm^{-2} (Ti:W atomic ratio = 1.7) and 0.77 TiO_2/0.80 WO_3 mg cm^{-2} (Ti:W atomic ratio = 2.8). Since bi-layer coatings are not uniform (see later) and possess 'cracked-mud' morphology, the thickness is expressed in mg cm^{-2}.

2.2 Microscopic and XRD characterization of coatings

Scanning electron microscopy (SEM) was carried out using a JEOL JSM 6390 microscope equipped with energy-dispersive spectroscopy (EDS) facility. X-ray diffraction (XRD) deposit characterization was performed with the help of a Philips automatic powder diffractometer (Bragg–Brentano arrangement, fixed slit mode) using Cu Kα-filtered radiation and scintillation registration.

2.3 Photoelectrochemical characterization of coatings and photoelectrolysis experiments

Photovoltammetry at small photoelectrodes was carried out with the Autolab 30 (EcoChemie) system, in a three-electrode cell equipped with a flat quartz window opposite the working electrode. The backside of the specimen (not facing the window) was insulated with epoxy resin so as not to contribute to the dark current. A saturated calomel electrode (SCE) was used as the reference electrode and a Pt foil as the counter electrode. Voltammograms were run for at least two consecutive times since preliminary experiments showed that a near-steady-state response was observed only after the second cycle; all the results reported correspond to the stabilized voltammetric picture. Photovoltammetry was performed between −0.4 V and +0.7 V vs. SCE. Photoamperometry experiments were conducted at +0.5 V vs. SCE. Tests were performed in 0.1 M Na_2SO_4 solution in the absence and presence of 4-CP using UV and visible lamps.

In 4-CP, photoelectrolysis experiments (performed at +0.5 V vs. SCE) a 500-mL cylindrical cell with a removable cap has been used. The UV or visible light lamp, placed in a cylindrical sleeve, was introduced from an opening in the middle of the cap leaving a solution available volume of 300 mL (filled with 250 mL of the 0.5 mM 4-CP solution to be treated). In each experiment, before UV or visible light irradiation, the solution and the catalyst were left in the dark for 60 min (as a reference point) until adsorption/desorption equilibrium was reached. The solution was then irradiated under UV or visible light. Samples of 5 mL were taken with the help of rubber tubing adjusted to a pipette. The mineralization of 4-CP was monitored by total organic carbon (TOC) analysis (TOC Shimadzu analyzer) and its degradation by spectrophotometry from the variation of the peak height at λ_{max} = 280 nm without control of the intermediate oxidation products. The rectangular (3 × 10 cm^2) electrodes were suspended from the cell cap and touched the cell wall leaving a 0.5-cm gap between the front electrode surface and the lamp sleeve and positioned at a 2.5-cm distance from the lamp (the backside of all electrodes was covered with a layer of insulating epoxy resin glue). A stainless steel wire was used as the counter electrode, and the reference electrode was a SCE electrode equipped with a salt bridge made of a thin thermoplastic tube ending to a Vycor® tip. The end of the tube was placed close to the upper edge of the photoelectrode to avoid obstruction of the incident light. A laboratory-made potentiostat was used for voltage application, interfaced to a PC for data collection via an18-bit AD card (Duo 18, WPI Inc.). Magnetic stirring was employed (at a stirring rate in the range where photodegradation was found to be independent of stirring).

Na_2SO_4 (Merck, pro analysi, >99%) was used as supporting electrolyte. 4-CP (Fluka, >98% (GC)) was the model organic pollutant. Doubly distilled water was used for the preparation of solutions.

A Radium Ralutec 9 W/78 UVA lamp (λ = 350–400 nm, λ_{max} = 366 nm), placed at a distance of 2.5 cm from the samples, was used for front face electrode illumination. A Radium Ralutec 9 W/71 visible light lamp (λ > 400 nm, λ_{max} = 437 nm) was used in corresponding experiments. The power density at the sample surface position was measured as 3 mW cm^{-2} with a photometer.

3 Results and discussion

3.1 Microscopic characterization of coatings

Figure 2a–f shows SEM back-scattered electron images (BEI) of all three tested bi-layer coatings at different magnifications, with increasing TiO_2 loadings from Fig. 2a, b to e, f.

Bright areas correspond to WO_3 and dark areas to TiO_2. This chemical contrast is due to the higher yield of electrons, backscattered by the element with a greater atomic mass (W). A 'cracked-mud' morphology is observed, characterized by 5–30 μm large patches or islands separated by cracks. Although the terraces of the islands are smoothened by the presence of a TiO_2 overlayer, these are also decorated by sparse nano-particles in the case of thicker samples (Fig. 2c–f), suggesting the preferred morphology of thicker TiO_2 layers. Hence, increasing the thickness of the deposits leads to increased roughness because of a nanoparticulate deposit growth. There is extensive mixing of WO_3 and TiO_2 (necessary for successful synergism), and TiO_2 pertains on island surfaces whereas WO_3 within the cracks, in accordance with Auger electron spectroscopy experiments

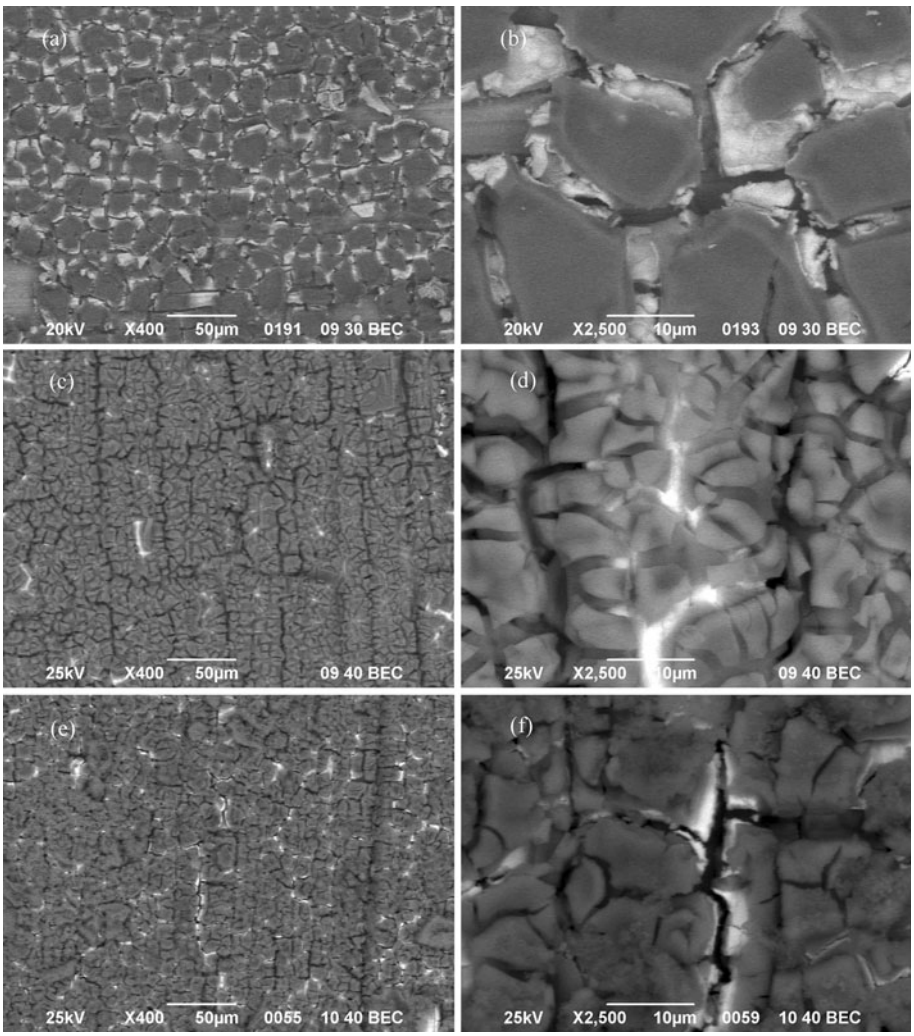

Fig. 2 SEM BEI images of bi-layer coatings on SS after annealing for 1 h at 400 °C: **a**, **b** 0.30 TiO_2/0.80 WO_3. **c**, **d** 0.40 TiO_2/0.70 WO_3. **e**, **f** 0.77 TiO_2/ 0.80 WO_3 mg cm^{-2}

presented in [23]. This open structure, where both components are exposed to light and the solution, is a prerequisite to a good photocurrent response under both UV and visible light illumination via synergy.

Obviously, the morphology is expected to be a very important factor especially in the case of visible light irradiation. Efficient visible light absorbance by WO_3 can only be considered if either the TiO_2 is thin enough to be transparent to visible light or microporous/particulate (at least at locations) as inferred from Fig. 2. These results are in harmony with our previous experiments with Auger electron spectroscopy [23].

3.2 Photoelectrochemical characterization of coatings and photoelectrolysis experiments

3.2.1 UV light irradiation

Figure 3a shows indicative CV curves in 0.1 M Na_2SO_4 under UV light illumination. Figure 3b presents similar voltammograms in the presence of 0.5 mM 4-CP. Pure TiO_2 film (0.80 mg cm^{-2}) is given for comparison. In all the cases, the current tends to a limiting value at the anodic potential limit at potentials higher than ca. +0.6 V, as expected for the *n*-type semiconductors of TiO_2 and WO_3. Also, in the case that the TiO_2 content is high enough (0.40, 0.77 mg cm^{-2}) with respect to WO_3, a second photocurrent wave is observed at lower potentials with an ill-defined plateau at ca. −0.2 V, most likely corresponding to that of pure TiO_2 [34]. For the thinnest TiO_2 film (0.30 mg cm^{-2}) as well as for pure WO_3, a single wave is observed. The obtained photocurrents seem to depend on the TiO_2 loading of the bi-layer coatings. The highest limiting photocurrent is observed at the thinnest sample with a catalyst ratio 0.30 TiO_2/0.80 WO_3 mg cm^{-2} (Ti:W atomic ratio = 1.1), in both cases. For higher thickness of the TiO_2 coatings, the photocurrent decreases. The lowest photocurrent is observed at the pure TiO_2 film.

The same trends can also be observed during rigorous constant potential photoamperometric experiments carried out at +0.5 V and depicted in Fig. 4a, b.

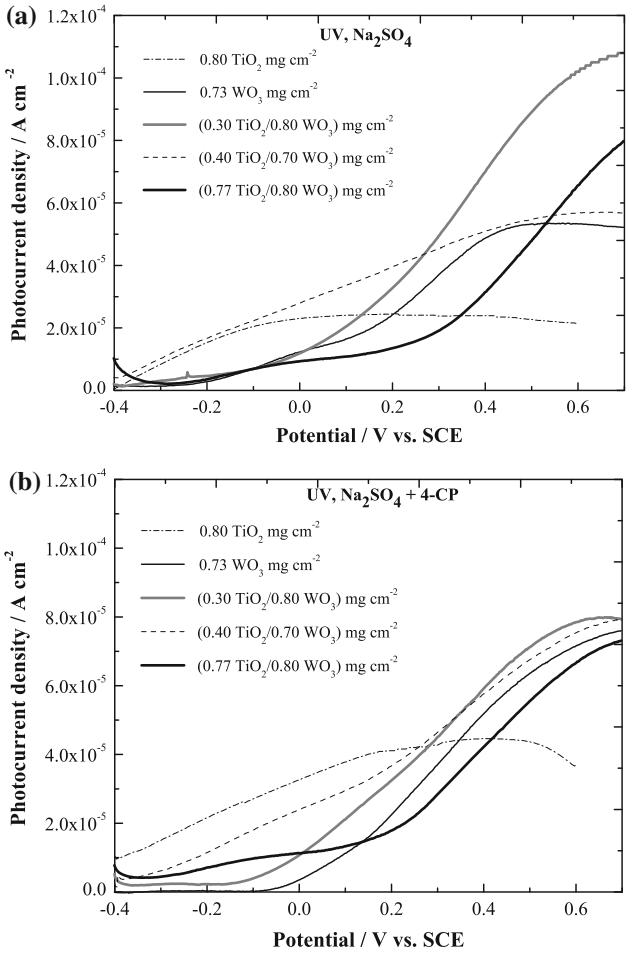

Fig. 3 **a** Photovoltammograms (10 mV s^{-1} potential scan rate; positive going sweep) in 0.1 M Na_2SO_4 solutions under UV illumination. **b** Photovoltammograms (10 mV s^{-1} potential scan rate; positive going sweep) in 0.1 M Na_2SO_4 + 0.5 mM 4-CP solutions under UV illumination

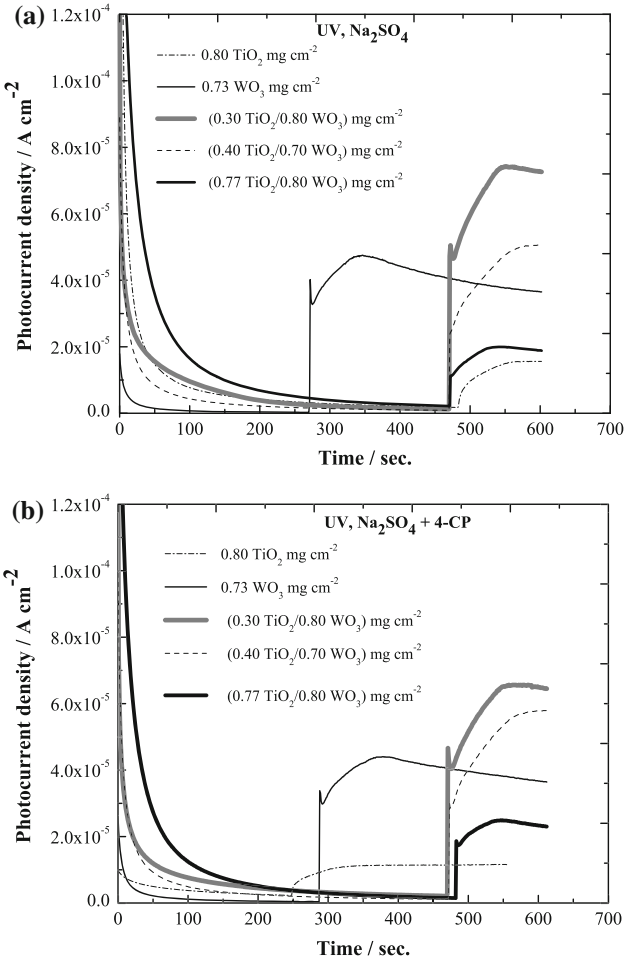

Fig. 4 **a** Photoamperometry curves at +0.5 V vs. SCE in 0.1 M Na_2SO_4 solutions under UV illumination. **b** Photoamperometry curves at +0.5 V vs. SCE in 0.1 M Na_2SO_4 + 0.5 mM 4-CP solutions under UV illumination

The lower photocurrents at the higher TiO_2 loadings can be explained by the fact that only part of the coating is irradiated, due to the relatively small penetration depth of UV light through TiO_2 and WO_3 (less than 1 μm). For example, the absorption length in TiO_2 is in the 0.25–0.1 μm range [34]. Holes and electrons are generated only in this part of the layer, and electrons have to cross the non-irradiated part of the layer (whose resistivity is higher than that of the irradiated part) to reach the conducting substrate and to be drawn away from the semiconductor.

One may also notice that the effect of 4-CP on the photocurrent is insignificant (comparison of Fig. 3a, b and 4a, b). This fact indicates that this species is not an efficient direct hole scavenger but, instead, it undergoes indirect photooxidation by $OH^{\bullet}$ radicals produced from hole scavenging by water molecules.

To further quantify the UV photoactivity of the photoelectrodes, the incident photon-to-current efficiencies (IPCEs; given by IPCE % = 100 × (1240 $i_{ph}/\lambda P$), where i_{ph} is the photocurrent at +0.5 V vs. SCE in mA cm^{-2}, λ the wavelength of the incident light in nm and P the incident light intensity in mW cm^{-2}) [40, 41] are given in Table 1. It is seen that the highest IPCE is found for the bi-layer electrode consisting of a thin TiO_2 film over the WO_3 underlayer.

Figure 5a, b shows the behaviour of larger samples during the constant potential bulk photoelectrocatalysis. The potential was kept constant at +0.5 V vs. SCE. The degradation of 4-CP was monitored by spectrophotometry (Fig. 5a) and its mineralization by total organic carbon (TOC) analysis (Fig. 5b). The photoelectrodes with catalyst composition 0.29 TiO_2/0.71 WO_3 and 0.45 TiO_2/0.76 WO_3 mg cm^{-2} exhibit superior 4-CP degradation and mineralization performance compared to the plain WO_3 and the thickest bi-layer photoelectrodes of 0.78 TiO_2/0.74 WO_3 mg cm^{-2}. This behaviour is in line with the photoelectrochemical behaviour of small samples under UV light illumination.

Table 1 Incident photon-to-current efficiency (IPCE, %) of TiO_2/SS, WO_3/SS and TiO_2/WO_3/SS photoelectrodes under UV light illumination in 0.1 M Na_2SO_4 solution without and with 0.5 mM 4-CP

	ICPE (%) (UV light)	
	Sulphate	4-CP
TiO_2/SS (0.80 mg cm^{-2} TiO_2)	2.6	4.9
WO_3/SS (0.73 mg cm^{-2} WO_3)	6.0	7.2
TiO_2/WO_3/SS (0.30 TiO_2/0.80 WO_3 mg cm^{-2})	10.0	8.0
TiO_2/WO_3/SS (0.40 TiO_2/0.70 WO_3 mg cm^{-2})	6.2	7.6
TiO_2/WO_3/SS (0.77 TiO_2/0.80 WO_3 mg cm^{-2})	5.4	6.3

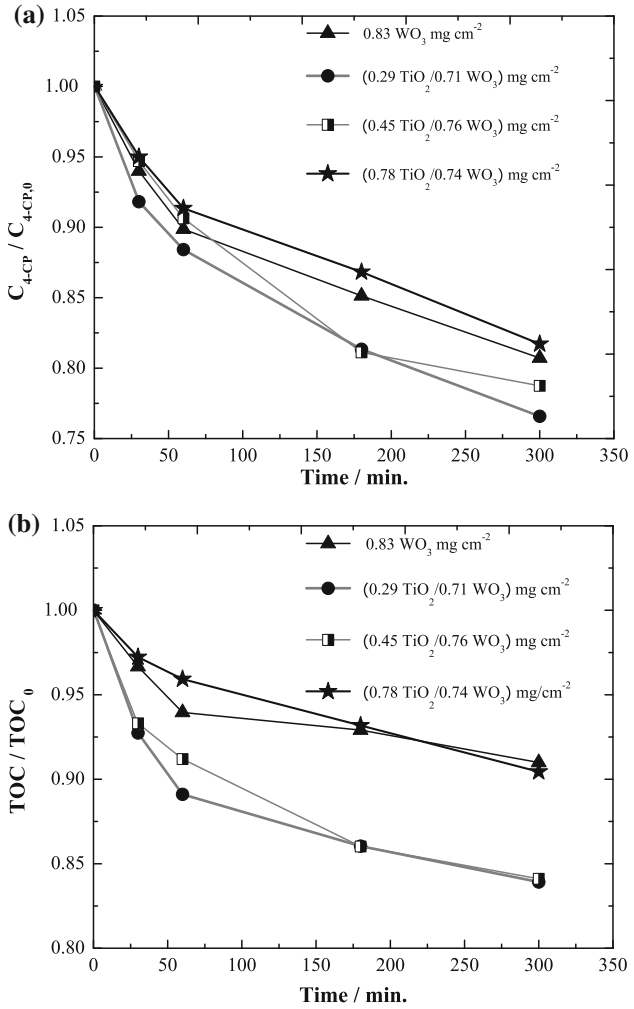

Fig. 5 **a** Variation of 4-CP concentration with time from 0.1 M Na_2SO_4 + 0.5 mM 4-CP 250 mL solutions, during constant potential (+0.5 V vs. SCE) photoelectrolysis at large (30 cm^2) electrodes, under UV light illumination, obtained by spectrophotometry. **b** Variation of 4-CP concentration with time from 0.1 M Na_2SO_4 + 0.5 mM 4-CP 250 mL solutions, during constant potential (+0.5 V vs. SCE) photoelectrolysis at large (30 cm^2) electrodes, under UV light illumination, monitored by TOC analysis

3.2.2 *Visible light irradiation*

Figure 6a, b present CV curves in 0.1 M Na_2SO_4 in the absence and presence of 0.5 mM 4-CP, respectively, under visible light illumination. Single wave photovoltammograms are obtained, since TiO_2 is not activated by itself but enhances the photoactivity of WO_3. Both in CV (Fig. 6a, b) and photoamperometry (Fig. 7a, b) experiments, the highest photocurrent is again at the samples with a catalyst loading ratio 0.30 TiO_2/0.80 WO_3 mg cm^{-2}.

During the bulk photoelectrocatalysis under visible light illumination the organic degradation and mineralization performance of all three bi-layer photoelectrodes is better than that of WO_3 but similar to each other, independently of their TiO_2 loading (Fig. 8a, b). Since under visible light only WO_3 can be excited and in our case the thickness of WO_3 is almost the same, probably this is the reason why

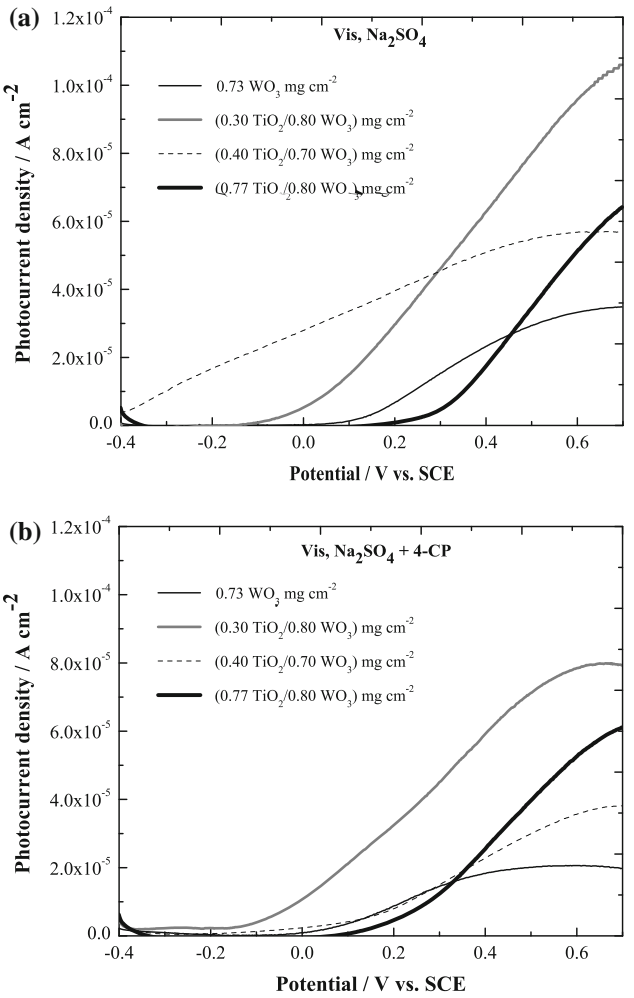

Fig. 6 **a** Photovoltammograms (10 mV s^{-1} potential scan rate; positive going sweep) in 0.1 M Na_2SO_4 solutions under visible light illumination. **b** Photovoltammograms (10 mV s^{-1} potential scan rate; positive going sweep) in 0.1 M Na_2SO_4 + 0.5 mM 4-CP solutions under visible light illumination

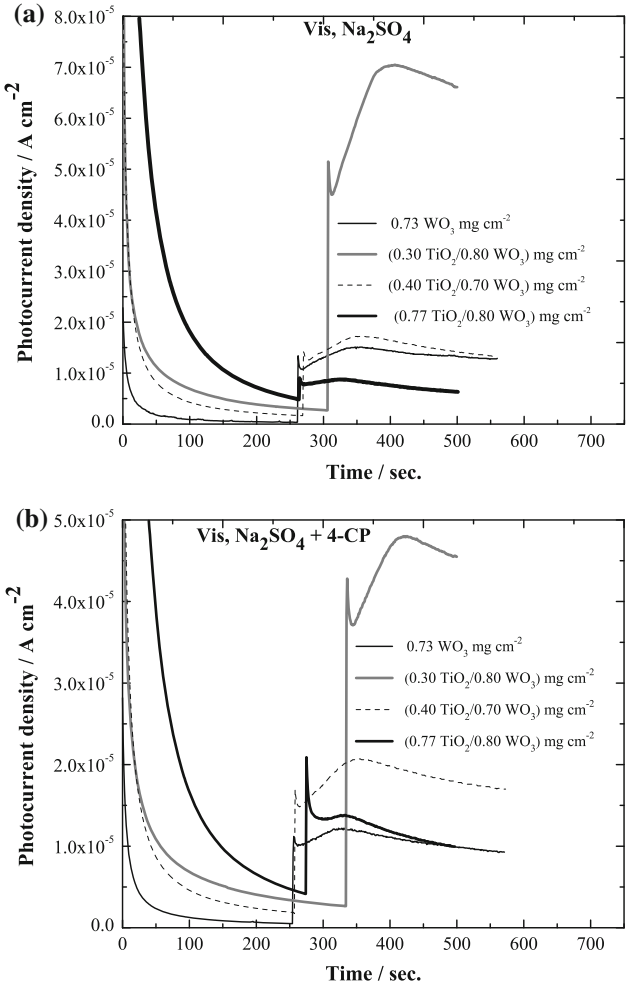

Fig. 7 **a** Photoamperometry curves at +0.5 V vs. SCE in 0.1 M Na_2SO_4 solutions under visible light illumination. **b** Photoamperometry curves at +0.5 V vs. SCE in 0.1 M Na_2SO_4 + 0.5 mM 4-CP solutions under visible light illumination

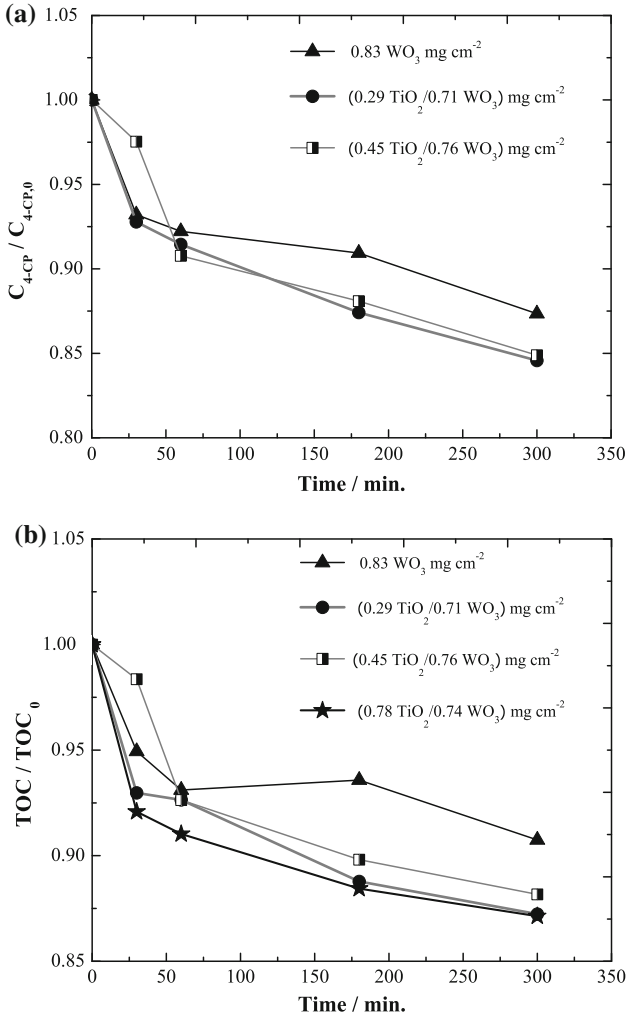

Fig. 8 **a** Variation of 4-CP concentration with time from 0.1 M Na_2SO_4 + 0.5 mM 4-CP 250 mL solutions, during constant potential (+0.5 V vs. SCE) photoelectrolysis at large (30 cm^2) electrodes, under visible light illumination, obtained by spectrophotometry. **b** Variation of 4-CP concentration with time from 0.1 M Na_2SO_4 + 0.5 mM 4-CP 250 mL solutions, during constant potential (+0.5 V vs. SCE) photoelectrolysis at large (30 cm^2) electrodes, under visible light illumination, monitored by TOC analysis

there is not a big difference in their behaviour. In other words under visible light the loading of TiO_2 (or total thickness of the samples) is not the determining factor for the photoelectrocatalytic activity of the bi-layer photoelectrodes since the effect of synergism occurs only at the TiO_2/WO_3 interface [25].

Comparing Figs. 7b and 8b an apparent difference with respect to the UV results (Figs. 4b 5b) can be noticed. The photocurrent trends cannot be related to the photodegradation trends. That is, despite the 0.30 TiO_2/0.80 WO_3 mg cm^{-2} sample showing the higher photocurrent, the same sample performs no better than the other bi-layer samples with respect to mineralization. This discrepancy should be traced in the complexity of the mechanism of visible excitation. It has been argued [25] that, since no holes are produced at TiO_2, electron transfer takes place from solution species to TiO_2 and, perhaps via a Ti(III)/Ti(II) transformation, to the photogenerated WO_3 holes. As the latter diffuse towards the TiO_2/WO_3 interface, recombination rates with photogenerated electrons in WO_3 are reduced, and the former create $OH^{\bullet}$ radicals at higher rates (if they react with water before they reach that interface), hence enhancing the photocatalytic activity of WO_3. Those holes that do reach the TiO_2/WO_3 interface combine with electrons provided from solution species to TiO_2 and diffusing through it. The latter process contributes also to the photocurrent, is expected to depend inversely on TiO_2 thickness/resistivity, but it is not guaranteed to lead to the formation of $OH^{\bullet}$ radicals and CP oxidation at the TiO_2 interface (oxidation of H_2O to O_2 could prevail). This mechanism could explain why the photocurrent increased

Table 2 Percentages of 4-CP mineralization under UV and visible light illumination

Loading (mg cm^{-2})	Mineralization of 4-CP (%) (TOC)	
	UV	Vis
0.83 WO_3	9.0	9.3
0.29 TiO_2/0.71 WO_3 (Ti:W atomic ratio = 1.2)	16.1	12.8
0.45 TiO_2/0.76 WO_3 (Ti:W atomic ratio = 1.7)	15.9	11.8
0.78 TiO_2/0.74 WO_3 (Ti:W atomic ratio = 3)	9.6	12.9

when TiO_2 became thinner but mineralization was not affected (since it occurred on the WO_3 part of the coating).

Table 2 summarizes the percentages of 4-CP mineralization for all the tested photoelectrodes both under UV and visible light illumination, in a 5-h period. It is seen that under visible light irradiation, the organic degradation performance of all the bi-layer photoelectrodes is close (bearing in mind the error of TOC analysis), independently of their total thickness (or the loading of TiO_2), whereas under UV light, the photoelectrocatalytic activity of the samples depends strongly on the total thickness of the coatings and the ratio between TiO_2 and WO_3. The best photoelectrocatalytic activity for photooxidation of 4-CP is shown by the bi-layer coating, with a loading of 0.29 TiO_2/0.71 WO_3 mg cm^{-2} (Ti:W atomic ratio = 1.2) under both UV and visible light irradiation.

The percentages of 4-CP mineralization obtained by TOC analysis are low, indicating the presence of organic compounds as intermediates in the solution. These values are in the range of values reported from Waldner et al. [40].

4 Conclusions

(i) In general, electrosynthesized bi-layer TiO_2/WO_3 coatings exhibit higher photoelectrocatalytic activity than plain single layer WO_3 coatings, both under UV and visible light illumination.

(ii) For the first time, the optimal atomic ratio between TiO_2 and WO_3 was found (Ti:W atomic ratio = 1.0–1.2) ensuring the best performance of electrosynthesized/electrodeposited photoelectrodes for photooxidation of 4-CP under both UV and visible light irradiation. This can be a good basis for further optimization of the photoelectrodes.

(iii) It was experimentally observed that under UV light illumination the ratio between TiO_2 and WO_3 or the total catalyst loading of bi-layer TiO_2/WO_3 coatings is the main factor affecting the photoelectrocatalytic activity. Under visible light irradiation, the thickness or loading of WO_3 should be sufficient for efficient light absorption. The morphology of the coatings is the other important factor. It has to be open or porous with the two semiconductor components homogeneously mixed, so that visible light can reach WO_3, and that a large WO_3/TiO_2 interface is formed.

Acknowledgement This study has been conducted within the frame of a NATO Science for Peace Project (SfP 982835).

References

1. Hoffmann MR, Martin ST, Choi W, Bahnemann DW (1995) Chem Rev 95:69
2. Fujishima A, Rao TN, Tryk DA (2000) J Photochem Photobiol C 1:1
3. Finklea HO (ed) (1998) Semiconductor electrodes. Elsevier, Amsterdam
4. Butterfield IM, Christensen PA, Hamnett A, Shaw KE, Walker GM, Walker SA, Howarth CR (1997) J Appl Electrochem 27:385
5. Candal RJ, Zeltner WA, Anderson MA (1998) J Adv Oxid Technol 3:270
6. Fernandez-Ibanez P, Malato S, Enea O (1999) Catal Today 54:329
7. Christensen PA, Curtis TP, Egerton TA, Kosa SAM, Tinlin JR (2003) Appl Catal B 41:371
8. Egerton TA, Christensen PA, Kosa SAM, Onoka B, Harper JC, Tinlin JR (2006) Int J Environ Pollut 27(1–3):2
9. Fraga LE, Anderson MA, Beatriz MLPMA, Paschoal FMM, Romão LP, Zanoni MVB (2009) Electrochim Acta 54(7):2069
10. Higashimoto S, Sakiyama M, Azuma M (2006) Thin Solid Films 503:201
11. Shang J, Yao W, Zhu Y, Wu N (2004) Appl Catal A 257:25
12. Ranjit KT, Willner I, Bossmann SH, Braun AM (2001) J Catal 204:305
13. Li FB, Li XZ, Ao CH, Lee SC, Hou MF (2005) Chemosphere 59:787
14. Uzunova M, Konstantinov M, Georgieva J, Dushkin C, Todorovsky D, Philippidis N, Poulios I, Sotiropoulos S (2007) Appl Catal B 73(1–2):23
15. He T, Ma Y, Cao Y, Hu X, Liu H, Zhang G, Yang W, Yao J (2002) J Phys Chem B 106:12670
16. Miyauchi M, Nakajima A, Watanabe T, Hashimoto K (2002) Chem Mater 14:4714
17. Shiyanovskaya I, Hepel M (1999) J Electrochem Soc 146:243
18. Luo J, Hepel M (2001) Electrochim Acta 46:2913
19. Pauporte Th, Goux A, Kahn-Harari A, Tacconi NR, Chenthamarakshan CR, Rajeshwar K, Lincot D (2003) J Phys Chem Solids 64:1737
20. Tacconi NR, Chenthamarakshan CR, Rajeshwar K, Pauporte T, Lincot D (2003) Electrochem Commun 5:220
21. Tacconi NR, Chenthamarakshan CR, Wouters KL, MacDonnell FM, Rajeshwar K (2004) J Electroanal Chem 566:249
22. Somasundaram S, Tacconi N, Chenthamarakshan CR, Rajeshwar K, Tacconi NR (2005) J Electroanal Chem 577:167
23. Georgieva J, Armyanov S, Valova E, Tsacheva Ts, Poulios I, Sotiropoulos S (2005) J Electroanal Chem 585:35
24. Somasundaram S, Chenthamarakshan CR, Tacconi NR, Basit NA, Rajeshwar K (2006) Electrochem Commun 8(4):539
25. Georgieva J, Armyanov S, Valova E, Poulios I, Sotiropoulos S (2007) Electrochem Commun 9:365
26. Bostt M, Jansses F (1998) Catal Today 2:429
27. Gillet M, Aguir K, Lemire C, Gillet E, Schierbaum K (2004) Thin Solid Films 467:239

28. Kopp L, Harmon BN, Liu SH (1977) Solid State Commun 22:677
29. Ohno T, Tanigawa F, Fujihara K, Izumi S, Matsumura M (1998) J Photochem Photobiol A 118:41
30. Santato C, Ulmann M, Augustynski J (2001) J Phys Chem B 105:936
31. Natarajan C, Nogami G (1996) J Electrochem Soc 143:1547
32. Hepel M, Hazelton S (2005) Electrochim Acta 50(25–26):5278
33. Kamada K, Mukai M, Matsumoto Y (2002) Electrochim Acta 47:3309
34. Georgieva J, Armyanov S, Valova E, Poulios I, Sotiropoulos S (2006) Electrochim Acta 51:2076
35. Georgieva J, Armyanov S, Valova E, Phillipides N, Poulios I, Sotiropoulos S (2008) J Adv Ox Tech 11(2):365
36. Vinodgopal K, Hotchandani S, Kamat PV (1993) J Phys Chem 97:9040
37. Mills A, Davies RH, Worsley D (1993) Chem Soc Rev 22:417
38. Kang Man Gu, Han Hyea-Eun, Kim Kang-Jin (1999) J Photochem Photobiol A 125:119
39. Hitchman ML, Tian F (2002) J Electroanal Chem 538–539:165
40. Waldner G, Pourmodjib M, Bauer R, Neumann-Spallart M (2003) Chemosphere 50:989
41. Krýsa J, Keppert M, Waldner G, Jirkovský J (2005) Electrochim Acta 50:5255